AD A138 381 STUDY OF THE INITIAL STAGES OF ANODIC OXIDATION OF POLYCRYSTALLINE SILVER IN KOH SOLUTIONS(U) BROOKLYN COLL NY DEPT OF PHYSICS M HEPEL ET AL. 31 JAN 84 TR-3 1/1

UNCLASSIFIED N00014-81-K-0399 F/G 7/4 NL

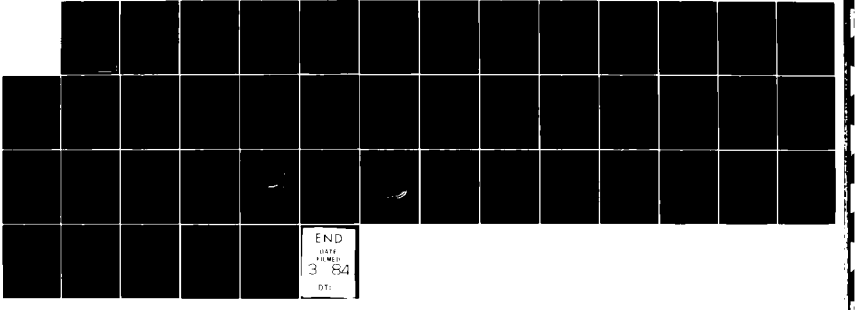

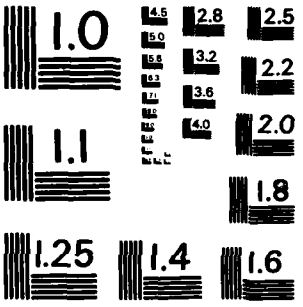

MICROCOPY RESOLUTION TEST CHART
NATIONAL BUREAU OF STANDARDS-1963-A

OFFICE OF NAVAL RESEARCH

Contract N00014-81-K-0399

Task No. NR - 628-765

TECHNICAL REPORT NO. 3

AD A138381

STUDY OF THE INITIAL STAGES OF ANODIC OXIDATION OF POLYCRYSTALLINE SILVER IN KOH SOLUTIONS

by

Maria Hepel and Micha Tomkiewicz

Accepted for Publication

in

Journal of the Electrochemical Society

Physics Department, Brooklyn College of CUNY
Brooklyn, N. Y. 11210

January, 1984

DTIC
ELECTE
FEB 2 9 1984
A

Reproduction in whole or in part is permitted for any purpose of the United States Government

This document has been approved for public release and sale; its distribution is unlimited

DTIC FILE COPY

84 02 22 069

SECURITY CLASSIFICATION OF THIS PAGE (When Data Entered)

REPORT DOCUMENTATION PAGE		READ INSTRUCTIONS BEFORE COMPLETING FORM
1. REPORT NUMBER 3	2. GOVT ACCESSION NO. AD-A138 38	3. RECIPIENT'S CATALOG NUMBER
4. TITLE (and Subtitle) STUDY OF THE INITIAL STAGES OF ANODIC OXIDATION OF POLYCRYSTALLINE SILVER IN KOH SOLUTIONS		5. TYPE OF REPORT & PERIOD COVERED
		6. PERFORMING ORG. REPORT NUMBER
7. AUTHOR(s) MARIA HEPEL MICHA TOMKIEWICZ		8. CONTRACT OR GRANT NUMBER(s) N00014-81-K-0399
9. PERFORMING ORGANIZATION NAME AND ADDRESS PHYSICS DEPARTMENT BROOKLYN COLLEGE OF CUNY BROOKLYN, N. Y. 11210		10. PROGRAM ELEMENT, PROJECT, TASK AREA & WORK UNIT NUMBERS NR-628-765
11. CONTROLLING OFFICE NAME AND ADDRESS OFFICE OF NAVAL RESEARCH/CHEMISTRY PROGRAM ARLINGTON, VIRGINIA 22217		12. REPORT DATE JANUARY 31, 1984
		13. NUMBER OF PAGES 36
14. MONITORING AGENCY NAME & ADDRESS(if different from Controlling Office)		15. SECURITY CLASS. (of this report) UNCLASSIFIED
		15a. DECLASSIFICATION/DOWNGRADING SCHEDULE

16. DISTRIBUTION STATEMENT (of this Report)
APPROVED FOR PUBLIC RELEASE AND SALE.
DISTRIBUTION UNLIMITED.

17. DISTRIBUTION STATEMENT (of the abstract entered in Block 20, if different from Report)

18. SUPPLEMENTARY NOTES
THIS PAPER IS ACCEPTED FOR PUBLICATION IN J. ELECTROCHEM. SOC.

19. KEY WORDS (Continue on reverse side if necessary and identify by block number)
ANODE, FILMS, NUCLEATION, TRANSIENTS, BATTERY

20. ABSTRACT (Continue on reverse side if necessary and identify by block number)
Growth of the anodic Ag_2O film on a polycrystalline silver disk electrode in 1 mol dm^{-3} KOH solution at ambient temperature has been examined using a variety of electrochemical techniques. On the basis of the experimental results, a solid-state model of silver electrode covered by a thin semiconductor film with a finite ionic conductivity has been proposed. It has been found, that under potentiostatic control, thickness of the oxide film adjusts very quickly to the hydrodynamic conditions by a deposition/dissolution process and the steady-state oxidation currents fulfil the Levich equation for RDE despite the fact that the

DD FORM 1 JAN 73 1473 EDITION OF 1 NOV 65 IS OBSOLETE
S/N 0102-LF-014-6601

SECURITY CLASSIFICATION OF THIS PAGE (When Data Entered)

SECURITY CLASSIFICATION OF THIS PAGE (When Data Entered)

electrode is covered by a thin Ag_2O film.

In the case of thicker films, after completion of nucleation and growth, changes in the hydrodynamic conditions do not influence the oxidation current and adjustment of the thickness of the oxide film to new hydrodynamic conditions proceeds at a slower rate because of the slowness of the solid-state diffusion step.

The Ag_2O nucleation and growth peak has been observed in chronoamperometric transients above potential of + 240 mV (vs. Ag/AgCl). It has been observed that the nucleation and growth peak decreases as the convective diffusion is accelerated by the rotation speed of the RDE. The dependence of the oxidation current upon the rotation speed vanishes gradually during the Ag_2O nucleation and growth process.

DTIC COPY INSPECTED 2

A-1

SECURITY CLASSIFICATION OF THIS PAGE (When Data Entered)

STUDY OF THE INITIAL STAGES OF ANODIC OXIDATION OF POLYCRYSTALLINE SILVER IN KOH SOLUTIONS

by

Maria Hepel and Micha Tomkiewicz

Department of Physics

Brooklyn College of CUNY

Brooklyn, NY 11210

Key words: anode, films , nucleation, transients, battery

ABSTRACT

Growth of the anodic Ag_2O film on a polycrystalline silver disk electrode in 1 mol dm^{-3} KOH solution at ambient temperature has been examined using a variety of electrochemical techniques. On the basis of the experimental results, a solid-state model of silver electrode covered by a thin semiconductor film with a finite ionic conductivity has been proposed. It has been found, that under potentiostatic control, thickness of the oxide film adjusts very quickly to the hydrodynamic conditions by a deposition/dissolution process and the steady-state oxidation currents fulfil the Levich equation for RDE despite the fact that the electrode is covered by a thin Ag_2O film.

In the case of thicker films, after completion of nucleation and growth, changes in the hydrodynamic conditions do not influence the oxidation current and adjustment of the thickness of the oxide film to new hydrodynamic conditions proceeds at slower rate because of the slowness of the solid-state diffusion step.

The Ag_2O nucleation and growth peak has been observed in chronoamperometric transients above potential of + 240 mV(vs. Ag/AgCl). It has been observed that the nucleation and growth peak decreases as the convective diffusion is accelerated by the rotation speed of the RDE. The dependence of the oxidation current upon the rotation speed vanishes gradually during the Ag_2O nucleation and growth process.

INTRODUCTION

The porous silver oxide electrodes in conjunction with zinc, cadmium, iron or hydrogen electrode serve as cathodes in various batteries (1). The silver electrodes offer excellent cycle life when used in rechargeable cells (1-4). In spite of development of commercial rechargeable silver-zinc batteries and the numerous investigations on the electro-oxidation of silver in alkaline solutions, the basic electrochemical processes involved are still not well understood. Apparently simple, consecutive oxidation scheme:

$$2\,Ag + 2\,OH^- = Ag_2O + H_2O + 2\,e^- \qquad [1]$$

$$Ag_2O + 2\,OH^- = Ag_2O_2 + H_2O + 2\,e^- \qquad [2]$$

is complicated by adsorption processes, nucleation overvoltages, solid-state diffusion and dissolution of Ag(I) in form of hydroxy-complexes. The resulting cyclic voltammogram for polycrystalline smooth electrode consists of five anodic peaks (see Figure 1) from which only two are associated with the formation of bulk Ag_2O and Ag_2O_2. Our present objective is to study the initial stages of the oxidation of smooth polycrystalline silver electrode.

Commencement of silver oxidation has been ascribed by Giles et al. (5,6) on the basis of impedance measurements, to its dissolution in form of $Ag(OH)_2^-$ complexes. According to Brezina et al. (7) the multilayer surface oxides are formed in the region of peak A_1 (see Figure 1), while Giles et al. (5,6) proposed a mechanism in which a monolayer of Ag_2O is completed in the region of the first oxidation peak. Droog et al. (8) and Ambrose et al. (15) treated their peak

as A_1 on the basis of the recalculation of the electrode potential scale, but previously (5,9,10) this peak was compared to the peak A_2 of other authors (11-14). Ambrose and Barradas (15) conclude on the basis of ring-disk study that in the A_1 region the dissolution of silver(I) as $Ag(OH)_2^-$ occurs giving linear Koutecky-Levich plots, $\underline{i}^{-1} = f(\omega^{-\frac{1}{2}})$. However, no further conclusions could have been drawn from the potential dependence of the determined values of the anodic current at $\omega \to \infty$. Earlier, the ring-disk technique has been applied by Miller (16). In this profound study the super-saturation in the vicinity of the electrode surface has been observed at the foot of the A_3 peak; the peaks A_1 and A_2 have not been observed on his freshly polished electrodes. Tilak et al. (9), Perkins et al. (10) and Stonehart (11) have treated the peak A_1 as an artifact (carbonate impurities, electrode etching, etc.). Droog et al. (8) attribute it to a complex situation in which at least two reactions are involved. They have proven that the change in carbonate concentration does not influence the A_1 peak potential. On the basis of the combined electrochemical and ellipsometric studies, the same authors (8) conclude that the A_1 peak is due to the silver dissolution and the formation of a surface monolayer. The peak A_2 has been identified by Dirkse and de Vries (12) as AgOH. To similar conclusions came Stonehart (11), neglecting dissolution of adsorbed and volume films of AgOH. Other hypotheses have also been proposed: oxidation of adsorbed hydrogen (13), preferential oxidation of surface silver atoms of low coordination number (16,17) and electrodissolution of silver with eventual formation of

a surface Ag_2O monolayer (9,10). The latter point of view has been associated (10) with the fact that no photo-effects were observed in the A_2 region. It has been found that the onset of the photocurrent on voltammetric characteristics for semiconducting n-Ag_2O film electrode takes place after the peak A_2 is completed (10,18).

The aging effects in the initially formed oxide film have been considered by Arvia and co-workers (19). The electrochemistry of silver in KOH solutions at elevated temperatures has been studied by Macdonald and co-workers (25-28).

In this study we examine the initial stages of the electro-oxidation of silver and growth of the semiconducting oxide films on polycrystalline silver electrodes in alkaline environment. The aim of this work is to describe the solid-state transport processes across the thin Ag_2O anodic film starting from first monolayers. The influence of different parameters on the total oxidation current is discussed. On the basis of the performed experiments, we propose a steady-state model of the Ag/Ag_2O electrode in the region of the space-charge build-up in the growing film. The LSV (linear scan voltammetry), LPSC (linear potential scan coulometry), CV (cyclic voltammetry) and RDE (rotating disk electrode) techniques have been used in measurements.

EXPERIMENTAL

A standard plexiglass electrolytic cell of about 100 cm^3 capacity was used in this study. A fritted glass tube was used to separate the

Pt-foil counter electrode from the main cell compartment. A silver rod (Johnson-Matthey) pressed into a teflon holder was used as a working electrode; its active surface area was 0.385 cm^2. A Model EC-219 rotating disk electrode (IBM Instruments, Inc.) was also used in experiments with controlled hydrodynamics. The potentials were measured against the double-junction silver/silver chloride electrode (Sargent-Welch Scientific Co.) with internal saturated KCl solution and external 1 mol dm^{-3} KNO_3 solution. The latter one was exchanged each day to avoid contamination of the main solution (KOH) by chloride ions.

A Model EG&G 173 potentiostat, equipped with a Model 179 digital coulometer and Model 175 universal programmer were used for voltammetric and chronocoulometric measurements. The experimental plots were recorded on a Hewlett-Packard Model 7044 A XY-plotter.

All the chemicals used were of analytical grade purity. The solutions were prepared with deionized water (18 M ohm) obtained using a Milli-Q purification system. Before the measurements, silver electrode was polished with 0.05 μm alumina (Fisher Scientific Co.), washed with deionized water and dried in a vacuum. The solutions were deoxygenated by nitrogen bubbling.

RESULTS

A well developed full CV characteristic for polycrystalline silver electrode in 1 mol dm^{-3} KOH solution can be obtained after approximately six cycles between -650 and +900 mV vs. Ag/AgCl reference electrode. Such a voltammogram is presented in Figure 1 for the potential

scan rate of 10 mV/s. All the Faradaic activity start at potentials positive to - 300 mu vs. Ag/AgCl. In consecutive cycles, only small changes (increase) in the peak heights are observed and they are due to increasing real surface area of the electrode. It is seen, that in the anodic scan, five current peaks are observed and they are designated A_1 through A_5. The current increase at the positive limit of the voltammogram is associated with the oxygen evolution reaction.

The formation of bulk Ag_2O and Ag_2O_2 can be ascribed (5,6,8-10, 12-21) to peaks A_3 and A_4, respectively. In the potential region of the peak A_5 at the foot of the oxygen evolution wave, the highest silver oxide, Ag_2O_3, is formed as has also been reported in Refs. (22,23,25, 29-32). The peaks A_1 and A_2 correspond to the initial stages of the silver oxidation.

When the electrode is conditioned in solution at open circuit for a long time (e.g., 24 hrs.) significant changes are seen in the LSV peak structure (Figure 2). The peak A_2 is not observed and the peak A_3 is much sharper than normally obtained on freshly polished electrode and also, it is higher than the peak A_4 corresponding to the nucleation and growth of the argentic oxide. Furthermore, upon successive cycles large changes are observed in the relative amplitude and the position of the various peaks. After about four cycles, a stable voltammogram emerges. This evolution is shown in Figure 2.

Potential region of the peak A_1

The current pre-wave A_1, hardly seen in Figure 1 is presented in enlarged scale in Figure 3 for a set of potential scan rates from 10 to 200 mV/s. When the anodic inversion potential E_i is equal +180 mV (as in Fig.3), a full anodic wave is developed only at $v \leqslant 10$ mV/s. In the cathodic scan, the peak C_1 is observed for all values of $\underline{v}$. The half-peak width increases with $\underline{v}$ and approaches approximately 60 mV at $\underline{v}$ = 200 mV/s. The dependence of the peak height upon the potential scan rate is presented in Figure 4.

The amount of charge consumed during LSV experiment can be calculated by integrating the voltammetric characteristic. The charge $\underline{Q}$ plotted $\underline{vs}$. the electrode potential gives then the LPSC characteristic. The same result can be obtained by the use of an electronic digital coulometer with analog output. Typical LPSC characteristics obtained in this way for the initial stage of silver oxidation, are presented in Figure 5. The experimental conditions are similar to the LSV curves shown in Figure 3, except that $\underline{E_i}$ is now equal to + 200 mV and the scan rates down to 1 mV/s are applied. Despite a fall of the LSV currents, the total anodic charge increases significantly as $\underline{v}$ decreases. The total cathodic charge $\underline{Q_C}$ does not compensate the anodic one $\underline{Q_A}$ and is always lower by about 1.2 - 1.5 times. The slower the potential scan, the larger the un-recovered charge.

Note, that all the charge peaks on the LPSC curves in Figure 5 appear exactly at the same potential. It corresponds to the iso-potential point $\underline{E_x}$ in the family of the respective LSV characteristics. In

this case $\underline{E}_x$ = 175 mV.

As shown by Droog et al. (8), the cathodic peak C_1 increases as the anodic potential limit $\underline{E}_i$ is shifted toward more positive values. We have observed the same effect on a stationary polycrystalline silver electrode. It is interesting now to compare this effect with the LSV curves obtained under different hydrodynamic conditions. A set of LSV characteristics with changing $\underline{E}_i$ obtained on the rotating silver disk electrode (RDE) is presented in Figure 6. No effect of $\underline{E}_i$ is observed up to $\underline{E}_i$ = 220 mV, unless fast potential scans are applied. The significance of this observation is discussed in the discussion section.

Dissolution effects in the formation of a thin Ag_2O film

The steady-state anodic oxidation currents measured on silver RDE at different angular velocities, in the potential range 180 - 250 mV, fulfil the Levich equation:

$$\underline{i} = 0.62 n F A D^{2/3} \nu^{-1/6} \omega^{1/2} (C_s - C^*) \qquad [3]$$

where D is the diffusion coefficient of the diffusing species, ν is the kinematic viscosity of the solution, C_s and C^* are the concentrations of the diffusing species at the electrode surface and in the solution bulk, respectively, ω is the angular velocity of the rotating disk and other symbols have their usual meaning.

The plot of the linear relations $\underline{i} = f(\sqrt{\omega})$ for different electrode potentials under steady-state conditions is presented in Figure 7. (The rotation speed $\overline{\omega}$ is expressed in r.p.m.; $\overline{\omega} = (60/2\pi)\omega$). It is evident from Figure 7 that the surface concentration C_s increases with

increasing potential up to approximately +250 mV. Above +250 mV the situation is much more complex because of commencement of the growth of the bulk Ag_2O film. This process proceeds via the nucleation and growth mechanism (21) with the control by a solid-state transport through the underlying basal layer.

The chronoamperometric curves presented in Figure 8 illustrate the nucleation and growth of Ag_2O film at $\underline{E}$ = +260 mV on RDE at 5990 r.p.m. and on a stationary electrode. Note, that the charge under the nucleation and growth peak is much greater for the stationary electrode than for the RDE. It is not unreasonable to assume that a thicker film is formed in the former case. The problem then arises what is the dependence of the oxidation current upon the hydrodynamic conditions in different stages of the Ag_2O film growth and what is the role of the oxide dissolution processes. From many experiments performed to answer this question, we present below three typical examples which explain the results in terms of the relaxation of the oxidation current after the perturbation of the transport rate in solution.

The current-time curve shown in Figure 9 was obtained after anodization of the silver disk electrode at constant potential $\underline{E}$ = +260 mV and $\omega = 0$ for 10 minutes until the nucleation and growth peak had been completed. This curve is a continuation of the curve 1 from Figure 8 . A very small response to the change of the hydrodynamic conditions is then observed (compare branch A obtained at $\omega = 0$ with branch B at ω= 5990r.p.m. in Fig.9) and the current returns to the previous value after stopping the disk rotation (branch C, $\bar{\omega} = 0$). However, a longer rotation at $\bar{\omega}$ = 5990 r.p.m. (branches

D and E) causes a gradual increase in the oxidation current which finaly approaches a steady-state level. If now the disk is stopped again, the current falls down but the nucleation and growth process starts again leading to the transient similar to that presented in Figure 10. The transients shown in Figure 10 illustrate the short-term rotation-speed dependence of the oxidation current in different stages of the Ag_2O film growth. Approximately steady-state anodic current at $\bar{\omega}$ = 5990 r.p.m. is observed after about 2 minutes (E = +260 mV). At the point A disk rotation was stopped. The $i - \bar{\omega}$ relations at different times (points B through G) are represented by the arrow whose length is equal to the difference Δi between the current at $\bar{\omega}$ = 5990 r.p.m. (measured after 25 sec) and the current at $\bar{\omega}$ = 0. Each arrow represents a separate experiment because the disk rotation for 25 sec. influences the nucleation and growth peak at $\bar{\omega}$ = 0 which becomes more expanded in time. As seen in Figure 10, the dependence of the oxidation current upon $\bar{\omega}$ vanishes gradually during the Ag_2O nucleation and growth process.

At the potential $\underline{E}$ = +230 mV, the nucleation and growth of the Ag_2O film is not observed and adjustment of the anodic current after changing rotation speed of the disk electrode proceeds faster. This situation is illustrated in Figure 11 and can be compared to those described above.

DISCUSSION

The voltammetric characteristics of silver electrodes in alkaline solutions are influenced by many factors from which the following seem to be the most important: (a) pre-treatment of the electrode surface, (b) roughness factor and surface structure, (c) hydrodynamic conditions, (d) solution impurities, (e) illumination and (f) electrode history (i.e., conditioning potentials, cycling, potential programs of previous experiments, etc.). Most of the present literature contradictions concerning silver oxidation can be explained when specific experimental conditions and procedures are taken into account.

The general oxidation path at the silver electrode in the potential range -300 through +900mV is shown in Fig.1 (cycling between -650 and +900mV). There are five anodic peaks A_1 through A_5. On the basis of our experiments, we list the conditions under which A_1 and A_2 peaks can be observed: unstirred solution, electrode roughned by strong oxidation and oxide stripping, solution not saturated with Ag(I) - - hydroxycomplexes. Similar peak structure has recently been reported by Droog,et.al. (8) and Teijelo,et.al. (except the feature A_5).

It is clear from our measurements (Figure 2,6) that the first two peaks A_1 and A_2 do not appear on the voltammogram for polycrystalline silver electrode conditioned for a long time or when the solution is stirred and is not saturated with Ag(I). The surface restructuring processes are evidently involved in the conditioning step. The reconstruction of the surface monolayers and formation

of the thermodynamically more stable atomic configurations with some preferential crystallographic orientations on a polycrystalline material can be considered. Eventually, it may concern even a few monolayers. Note, that some authors (14, 17) identify the peak A_2 with the preferential oxidation of surface atoms of low coordination number. Also, in this case (Figure 2, curve 1) the peak A_3 has a different shape than that seen in Figure 1; it is sharp and much higher than the peak A_4 for the Ag_2O_2 nuclation and growth.

This indicates that Ag_2O nucleation process (A_3) is highly retarded on reconstructed surfaces and starts spontaneously when the solution becomes supersaturated at the electrode surface and the potential reaches sufficiently positive value. Before the first monolayer of Ag_2O film starts to grow, the reaction of silver dissolution according to Giles and Harrison(5) can be represented by the equation:

$$Ag + 2\,OH^- = Ag(OH)_2^- + e^- \qquad [4]$$

assumed also by other authors (15).

The initial stage of Ag_2O formation proceeds via the net electrochemical reaction [5] which in our opinion is presumably composed from a few elementary steps:

$$2\,Ag + 2\,OH^- - 2\,e = Ag_2O_{(i)} + H_2O \qquad [5]$$

or by the precipitation mechanism which is generally accepted for thicker Ag_2O films (9, 15, 16, 21, 22). In the latter case the reactions that might be involved are the following:

$$2\,Ag(OH)_2^- = Ag_2O_{(i)} + 2\,OH^- + H_2O \qquad [6]$$

$$2\,AgO^- + H_2O = Ag_2O_{(i)} + 2\,OH^- \quad [7]$$

$$2\,AgOH_{(aq)} = Ag_2O_{(i)} + H_2O \quad [8]$$

The subscript (i) was used at Ag_2O in the reaction equations [5] - -[8] to denote differences betweeen consecutive monolayers (at least between the first, adsorbed layer and the bulk Ag_2O layers). The complexes $Ag(OH)_2^-$ and AgO^- are prevailing Ag(I) species in the solution (16, 32). The reaction equation [5] has been proposed for the formation of the adsorption Ag_2O film (5). For the next monolayers, the same equation can be used as a total reaction for the film growth, but it has been found on the basis of the RRDE experiments (15,16),that the important step in the mechanism is precipitation of Ag_2O from the super-saturated solution via the nucleation and growth process. Dignam et al.(33) and other authors (9, 21, 34) pointed out the significance of the solid-state mass transport in the Ag_2O film formation.

Initial stages of silver oxidation

Determination of the contributions of the initial silver dissolution process and the Ag_2O adsorption reaction to the total current is difficult because no mechanistic studies have been performed which could give a better insight into the reactions involved.

Comparison of our LSV characteristics for the region of peak A_1 (Figure 3 and 6) shows a significant influence of the dissolution processes at the RDE where the effect of the increasing inversion potential E_i on the cathodic currents is not observed. The results of the

LPSC measurements (Figure 5) at a stationary electrode can be explained by loss of charge due to the dissolution at $\underline{E}_i < 200\,mV$.

On the basis of the RDE experiments (Figure 7 and other data) we can calculate the surface concentration C_s of the Ag(I) species at different potentials using Levich equation [3]. For a reversible electrodissolution of metallic silver, one can expect a linear relation $\log C_s$ vs. potential $\underline{E}$ with a slope $(\delta \underline{E} / \delta \log C_s) = 59.16\,mV$. However, in our case (Figure 12) the slope is 73 mV at higher potentials and about 90 mV at lower potentials. The potential region where the slope 73 mV is observed, corresponds to the region of the change in optical parameters ($\delta\Delta$) in the ellipsometric studies of Droog et al.(8) and can be associated with the influence of the adsorption process.

Effect of the solid-state transport and nucleation and growth phenomena on the potentiostatic transients under different hydrodynamic conditions

At potentials $\underline{E} > 250\,mV$, the bulk Ag_2O is formed, however, the Ag(I) surface concentration C_s maintains the saturation value. The dependence of the steady-state oxidation currents vs. $\sqrt{\omega}$ is still similar to that represented by the curve for $\underline{E} = 250\,mV$ although adjustment of the film thickness during the change in the rotation speed takes place (Figures 9-11). This fact seems to be a natural consequence of the interrelations between the varying rate of convective diffusion in the solution and the mass transport within the solid film. The electrical conductivity of Ag_2O is very low ($\sigma = 10^{-8}$ S/cm (33)) and, basically, one might assume a constant field

approximation:

$$\underline{E} = -\frac{d\phi}{dx} = \text{const} \qquad (9)$$

for the potential distribution across the Ag_2O film, similarily as for example for niobium oxide (35) or iron oxides (36). In consequence adjustment of the film thickness to the changed hydrodynamic conditions would require in this case a change in the potential drop across the film. But, because of the observed constancy of $C_s = C_s^{sat}$ at varying $\bar{\omega}$ (i.e., linearity of the Levich plot) under steady-state conditions, it seems that constant potential drop rather than constant field is maintained in the oxide film. Work is underway in our laboratory to address this question, using impedance measurements, and the results will be reported in the forthcoming publications.

And finally, we would like to emphasize one characteristic feature of the system behavior: the invariance of the LSV peak curents A_2 and A_3 with respect to the rotation speed ω as was reported by Tilak et. al. (8) and Hampson et. al. (17) as compared to the rotation speed dependence of the oxidation currents at constant potentials in the potential region of the LSV peak A_2 that is reported here (Figures 8 - 11). Possible explanation of this fact is that in the LSV experiments (v = const), the film thickness increases following the continuous changes in the electrode potential. In the case of the nucleation and growth, the current peak is determined by the increasing real surface area. An acceleration of the rotation speed causes a longer dealy before the commencement of the nucleation and growth process and this is manifested by a shift of the peak potential. The

peak currents, however, remain undisturbed by the dissolution processes. The nucleation and growth peaks seen in Figures 8 and 10 correspond probably to the same processes as those at the LSV peak A_3 because a further potential scan applied in the direction of positive potentials shows only peak A_4 (Ag_2O_2 formation).

CONCLUSION

The steady-state oxidation currents measured on the polycrystalline silver RDE fulfill the limiting Levich equation despite the fact that the electrode is covered by a thin Ag_2O film. When the hydrodynamic conditions are changed by the change of the rotation speed of the disc, the anodic current adjusts to the new value. The rate of this adjustment indicates that the solid-state transport processes and changes in the film thickness are involved. However, the final value of the current indicates that the saturation of the solution with respect to Ag(I) is maintained. A steady-state model of the metal/semiconductor electrode undergoing dissolution is thus proposed. In the case of thick Ag_2O films, the solid-state diffusion control of the anodic processes can occur. At the same constant electrode potential, thicker films are obtained under conditions of slower mass transport in the solution. This conclusion follows from the proposed model and is consistent with the experimental results.

The Ag_2O nucleation and growth peak has been observed in chronoamperometric transients above the potential of + 240 mV(vs. Ag/AgCl). The height of this peak decreases as the convective diffusion is accelerated by the rotation speed of the RDE.

In case of the monolayer Ag_2O films, which can be obtained in the potential region of the first LSV peak (A_1), the surface concentration of Ag(I) in solution is lower than the equilibrium value corresponding to the reversible Ag/Ag(I) electrode and the slope ($\delta \underline{E} / \delta \log \underline{C}_s$) is greater than 59.16 mV. The results of the LPSC measurements obtained on a stationary silver disk electrode show a large un-recovered charge during the potential cycle (starting from the negative potential limit at the conditioning potential). The dependence of the peak currents A_1 and C_1 upon the potential scan rate is not linear. All these observations indicate a complex behavior of the system in the region of peak A_1 which cannot be simply described by the equilibrium silver dissolution with the formation of a reversible adsorption layer of Ag_2O.

Acknowledgement

This work was supported by the Office of Naval Research under the Contract N00014-81-K-0339.

References

1. S.U. Falk and A.J. Salkind, Alkaline Storage Batteries, John Wiley & Sons, 1969.

2. P. O'D. Offenhartz and G.L. Holleck, J. Electrochem. Soc. 127, 1213 (1980).

3. R. Serenyi, Extended Abstracts, Electrochemical Society Fall Meeting, Detroit, 1982.

4. H.A. Frank, W.L. Long and A.A. Uchiyama, J. Electrochem. Soc., 123, 1 (1976).

5. R.D. Giles and J.A. Harrison, J. Electroanal. Chem., 27, 161 (1970).

6. R.D. Giles, J.A. Harrison and H.R. Thirsk, J. Electroanal. Chem., 22, 375 (1969).

7. M. Brezina, J. Koryta and M. Musilová, Collect. Czech. Chem. Commun., 33, 3397 (1968).

8. J.M.M. Droog, P.T. Alderliesten and G.A. Bootsma, J. Electroanal. Chem., 99, 173 (1979).

9. B.V. Tilak, R.S. Perkins, H.A. Kozlowska and B.E. Conway, Electrochim. Acta, 17, 1447 (1972).

10. R.S. Perkins, B.V. Tilak, B.E. Conway and H.A. Kozlowska, Electrochim. Acta, 17, 1471 (1972).

11. P. Stonehart, Electrochim. Acta, 13, 1789 (1968).

12. T.P. Dirkse and D.B. de Vries, J. Phys. Chem., 63, 107 (1959).

13. T.G. Clarke, N.A. Hampson, J.B. Lee, J.R. Morley and B. Scanlon, Can. J. Chem., 46, 3437 (1968).

14. T.G. Clarke, N.A. Hampson, J.B. Lee, J.R. Morley and B. Scanlon, Ber. Bunsenges. Phys. Chem., 73, 279 (1969).

15. J. Ambrose and R.G. Barradas, Electrochim., Acta, 19, 781 (1974).

16. B. Miller, J. Electrochem. Soc., 117, 491 (1970).

17. N.A. Hampson, K.I. MacDonald and J.B. Lee, J. Electroanal. Chem., 45, 149 (1973).

18. R. Memming, F. Möllers and G. Neumann, J. Electrochem. Soc., 117, 451 (1970).

19. M.L. Teijelo, J.R. Vilche and A.J. Arvia, J. Electroanal. Chem., 131, 331 (1982).

20. M. Fleischamnn, D.J. Lax and H.R. Thirsk, Trans. Faraday Soc., 64, 3137 (1968).

21. M. Fleischmann, D.J. Lax and H.R. Thirsk, Trans. Faraday Soc., 64, 3128 (1968).

22. E.J. Casey and W.J. Moroz, Can. J. Chem., 43, 1199 (1965).

23. B.E. Conway and M.A. Sattar, Electrochim. Acta, 14, 695 (1969).

24. P. Stonehart and F.P. Portante, Electrochim. Acta, 13, 1805 (1968).

25. B.G. Pound, D.D. Macdonald and Y.W. Tomlinson, Electrochim. Acta, 24, 929 (1979).

26. B.G. Pound, D.D. Macdonald and Y.W. Tomlinson Electrochim. Acta, 25, 563 (1980).

27. B.G. Pound, D.D. Macdonald and Y.W. Tomlinson, Electrochim. Acta, 25, 1293 (1980).

28. B.G. Pound, D.D. Macdonald and Y.W. Tomlinson, Electrochim. Acta, 27, 1489 (1982).

29. B.D. Cahan, Y.B. Ockerman, R.F. Amlie and P. Rüetschi, J. Electrochem. Soc. 107, 725 (1960).

30. Y.A. McMillan, Chem. Rev., 62, 65 (1962).

31. Yu.S. Gorodetskii, Elektrochimiya, 1, 681 (1965).

32. Yu. V. Pleskov, Dokl. Akad. Nauk SSSR, 117, 645 (1957).

33. M.J. Dignam, H.M. Barrett and G.D. Nagy, Can. J. Chem. 47I, 4253 (1969).

34. B.N. Kabanov and D.I. Leikis, Z. Elekrochem., 62, 660(1958).

35. L. Young, Trans. Faraday Soc., 51, 1250(1955).

36. B.D. Cahan and Chia-Tien Chen, J. Elektrochem. Soc., 129, 921 (1982).

37. A.A. Yakovleva, T.I. Borisova and V.I.Veselovskii, Russian J. Phys. chem., 36, 763(1962).

38. G. Bush, Uspekhi Fiz. Nauk, 47, 2(1952).

39. L. Bergman and J. Hansler, Z. Physik, 1-2, 100(1936).

FIGURE CAPTIONS

Figure 1. The CV characteristic for the polycrystalline silver electrode (geometric area A = 0.385 cm^2) in 1 mol dm^{-3} KOH solution at 22 °C. Potential cycles 6-8 between -650 and +900 mV vs. Ag/AgCl, $\underline{v}$ = 10 mV/s, quiet solution, $\underline{E}_{cond}$ = -1240 mV.

Figure 2. Consecutive runs (1 to 4) of the cyclic voltammogram for a stationary silver electrode conditioned for 24 hours in 1 mol dm^{-3} KOH solution. Scan rate: 10 mV/s, potential limits; -650 and +900 mV, A = 0.385cm^2.

Figure 3. The LSV characteristics for the Ag electrode in 1 mol dm^{-3} KOH solution in the region of peaks A_1 and C_1 for the potential scan rate $\underline{v}$[mV/s]: (1)10, (2)20, (3)40, (4)60, (5)80, (6)100, (7)120, (8)140, (9)160, (10)180, (11)200, A = 0.385cm^2.

Figure 4. The dependence of the cathodic peak current (C_1) upon the potential scan rate (curve 1) and the square root of the scan rate (curve 2). Solution: 1 mol dm^{-3}.

Figure 5. The LPSC curves for the initial stage of silver oxidation and reduction in 1 mol dm^{-3} KOH solution. Potential scan rates $\underline{v}$[mV/s]: (1)200, (2)180, (3)160, (4)140, (5)120, (6)100, (7)80, (8)60, (9)40, (10)20, (11)10, (12)5, (13)2, (14)1, A = 0.385cm^2.

Figure 6. The slow-scan, LSV characteristics for a rotating polycrystalline silver disk electrode in 1 mol dm^{-3} KOH solution for different values of the anodic inversion potential $\underline{E}_i$ [mV]: (1)175, (2)182, (3)190, (4)200, (5)210, (6)220. Conditions: $\underline{v}$ = 1 mV/s, ω = 5990 r.p.m.

Figure 7. Dependence of the steady-state oxidation current i_d upon the square root of the rotation speed $\sqrt{\omega}$ (in: $(r.p.m.)^{\frac{1}{2}}$) of the silver RDE for different electrode potentials E [mV vs. Ag/AgCl]: (1)260, (2)250, (3)230, (4)200, (5)180. Solution: 1 mol dm^{-3} KOH.

Figure 8. Typical chronoamperometric transients obtained on a stationary (1) and rotating (2) silver disk electrodes at E = +260 mV (vs. Ag/AgCl) in 1 mol dm^{-3} KOH solution. Curve 2: ω = 5990 r.p.m.
Current scale: right for curve 1, left for curve 2.

Figure 9. The current - time transient obtained on a silver disk electrode after depositing of the Ag_2O film for τ_d = 600 s. The branches A-E of the transient correspond to the rotation speed of the disk ω: (A,C)0 and (B,D,E)5990 r.p.m. Solution: 1 mol dm^{-3} KOH; E = +260 mV (vs. Ag/AgCl), geometric area A = 0.192 cm^2.

Figure 10. The short-term effect (marked by the length of arrows) of changing the rotation speed of the filmed silver disk electrode from 0 to 5990 r.p.m. in different stages of the Ag_2O film growth. The current - time transients were obtained at ω = 5990 r.p.m. (branch A) and 0 r.p.m. (branch B). Each arrow represents a separate experiment in which the transient was interrupted at the time (marked by arrow) by turning the rotation on (ω = 5990 r.p.m.) and reading the value of current after 25 sec. E = 260 mV (vs. Ag/AgCl), geometric area A = 0.192 cm^2.

Figure 11. The current response on the change in the rotation speed of the filmed polycrystalline silver disk electrode at E = 230 mV (vs. Ag/AgCl) in 1 mol dm^{-3} KOH solution; ω [r.p.m.]: (1)0, (2)5990, (3)0, (4)100, (5)400, (6)900, (7)1600, (8)2500, (9)3600, (10)4900, (11)5990. Dashed curve: initial current - time transient at 5990 r.p.m. (current

scale x2).

Figure 12. Plot of the elctrode potential vs. the logarithm of the surface Ag(I) concentration calculated from experimental steady-state oxidation currents using Levich equation (3). Solution: 1 mol dm^{-3} KOH.

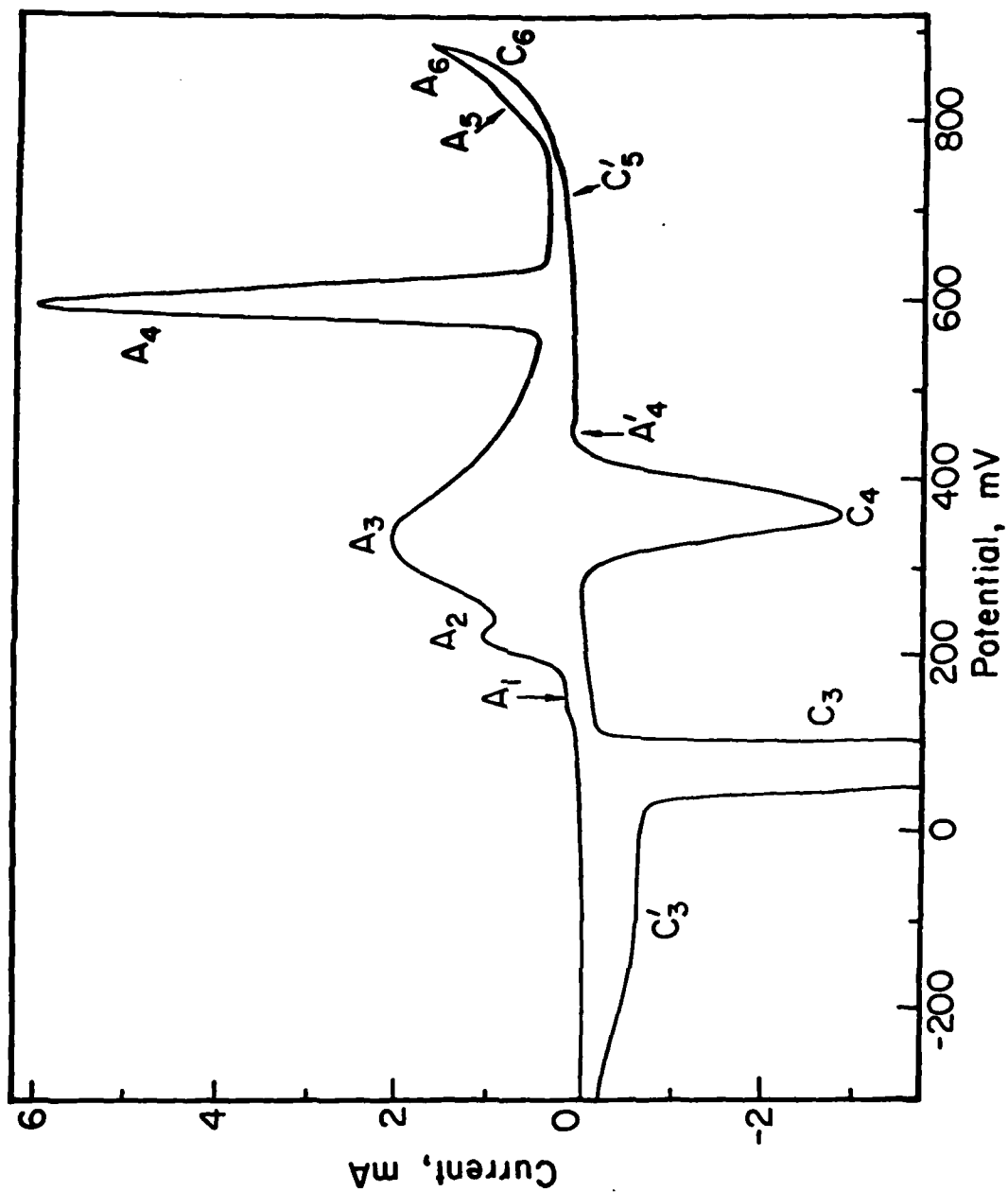
Current, mA
6
4
2
0
-2
-200
0
200
400
600
800
Potential, mV
A6
C6
A5
C'5
A4
A'4
C4
A3
A2
A1
C3
C'3

Fig. 1

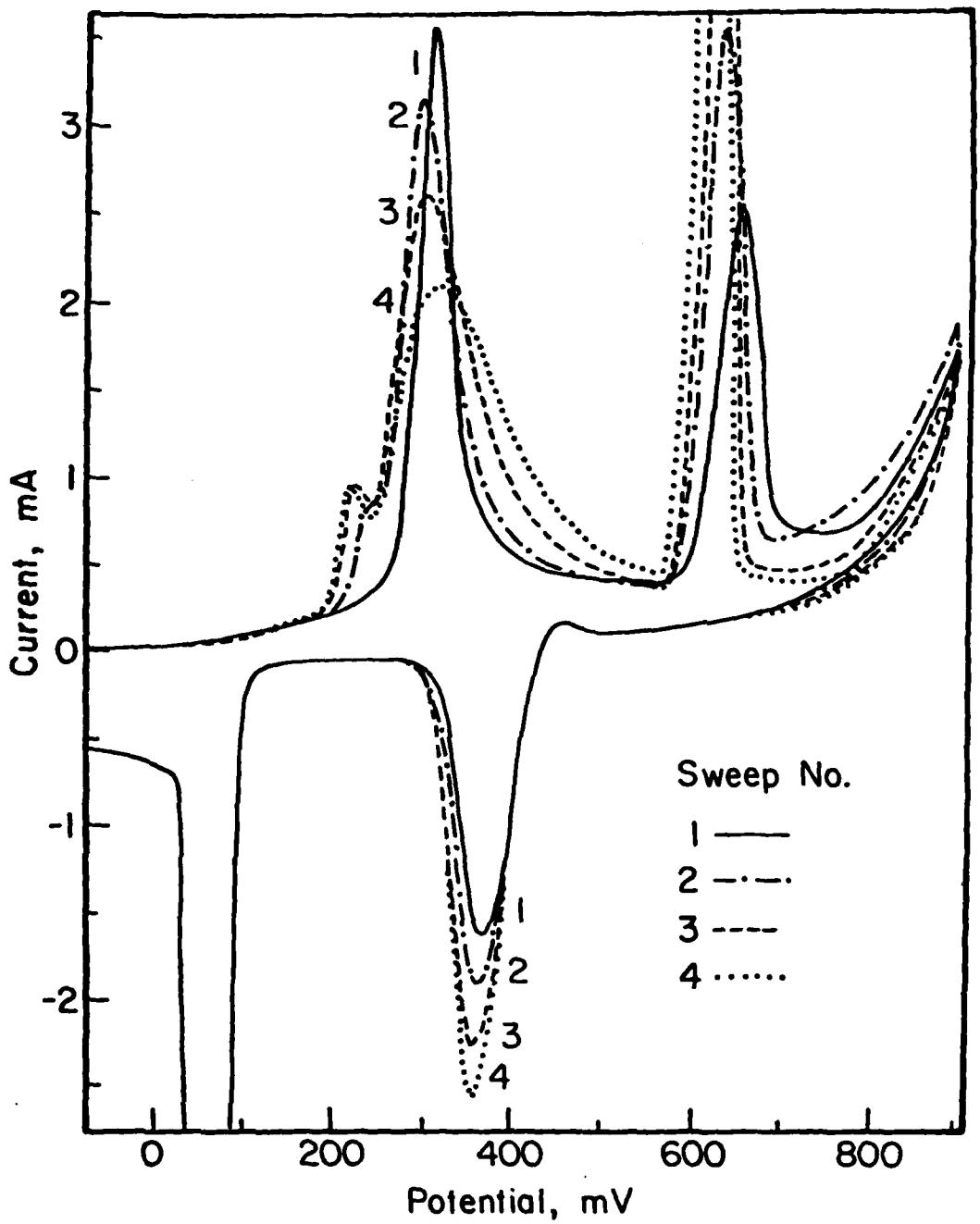
Current, mA
3
2
1
0
-1
-2
0
200
400
600
800
Potential, mV
1
2
3
4
Sweep No.
1
2
3
4

Fig. 2

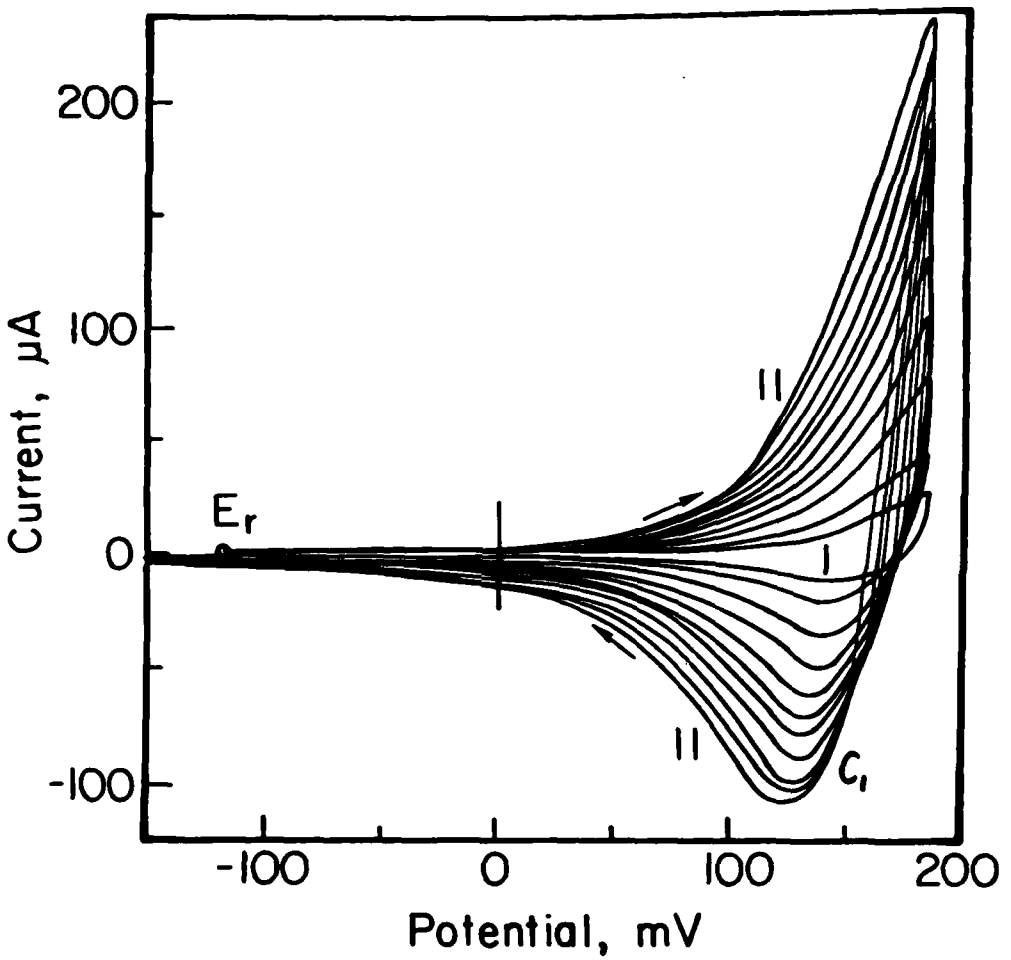

Fig. 3.

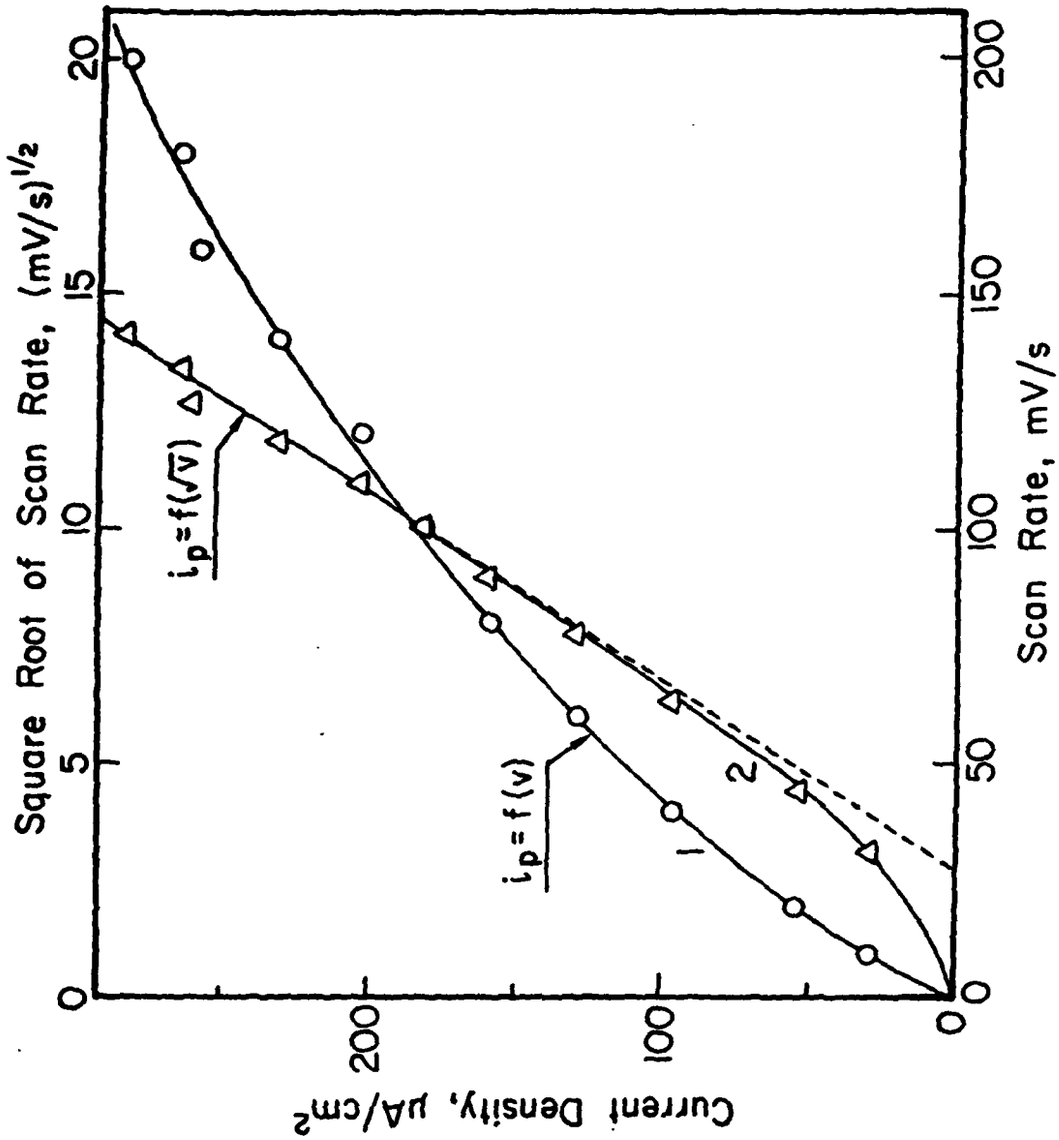
Square Root of Scan Rate, (mV/s)$^{1/2}$
Scan Rate, mV/s
Current Density, μA/cm^2
$i_p = f(\sqrt{v})$
$i_p = f(v)$
1
2
0
5
10
15
20
50
100
150
200

Fig. 4

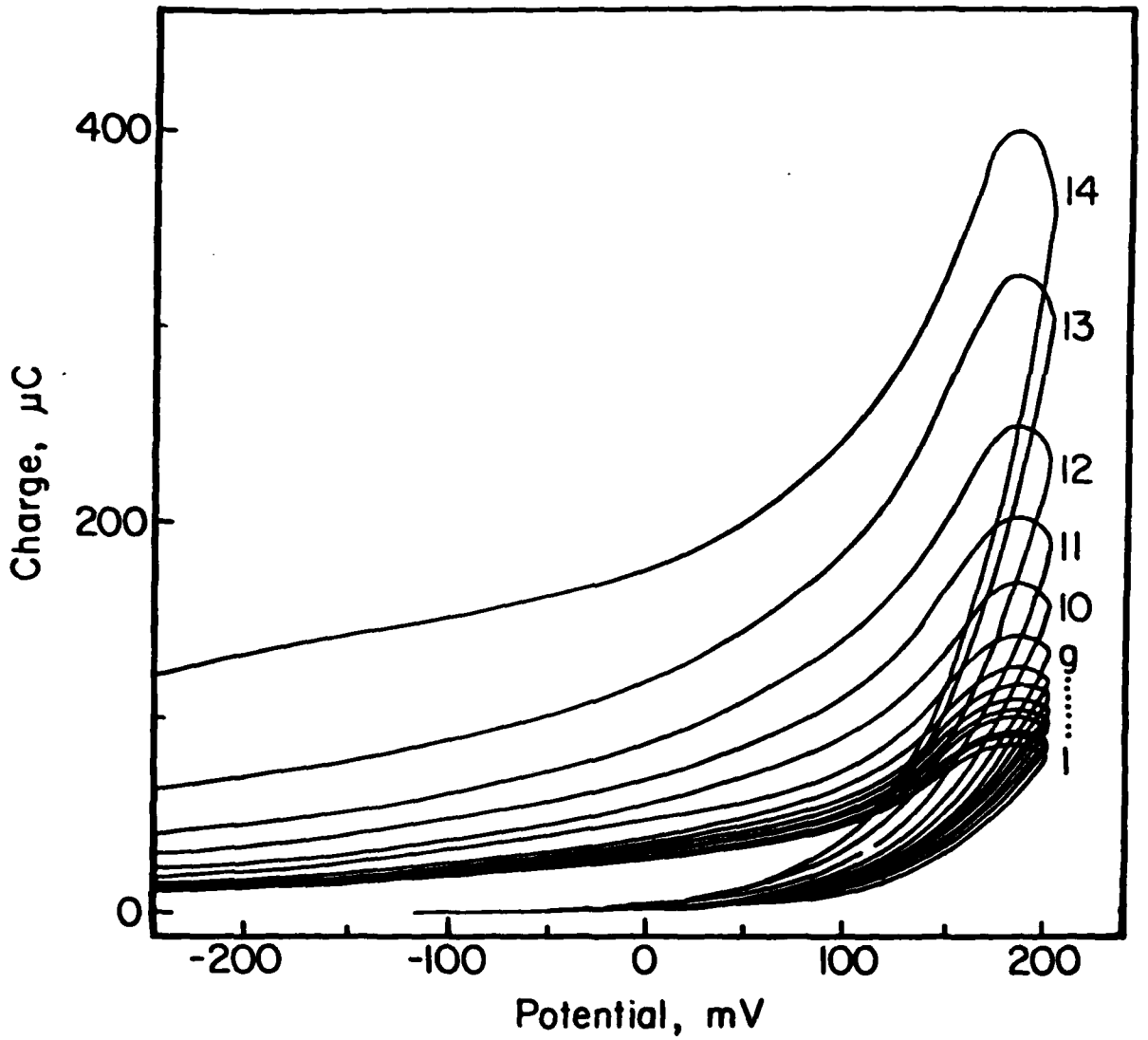
400
200
0
Charge, μC
14
13
12
11
10
9
1
-200
-100
0
100
200
Potential, mV

Fig. 5

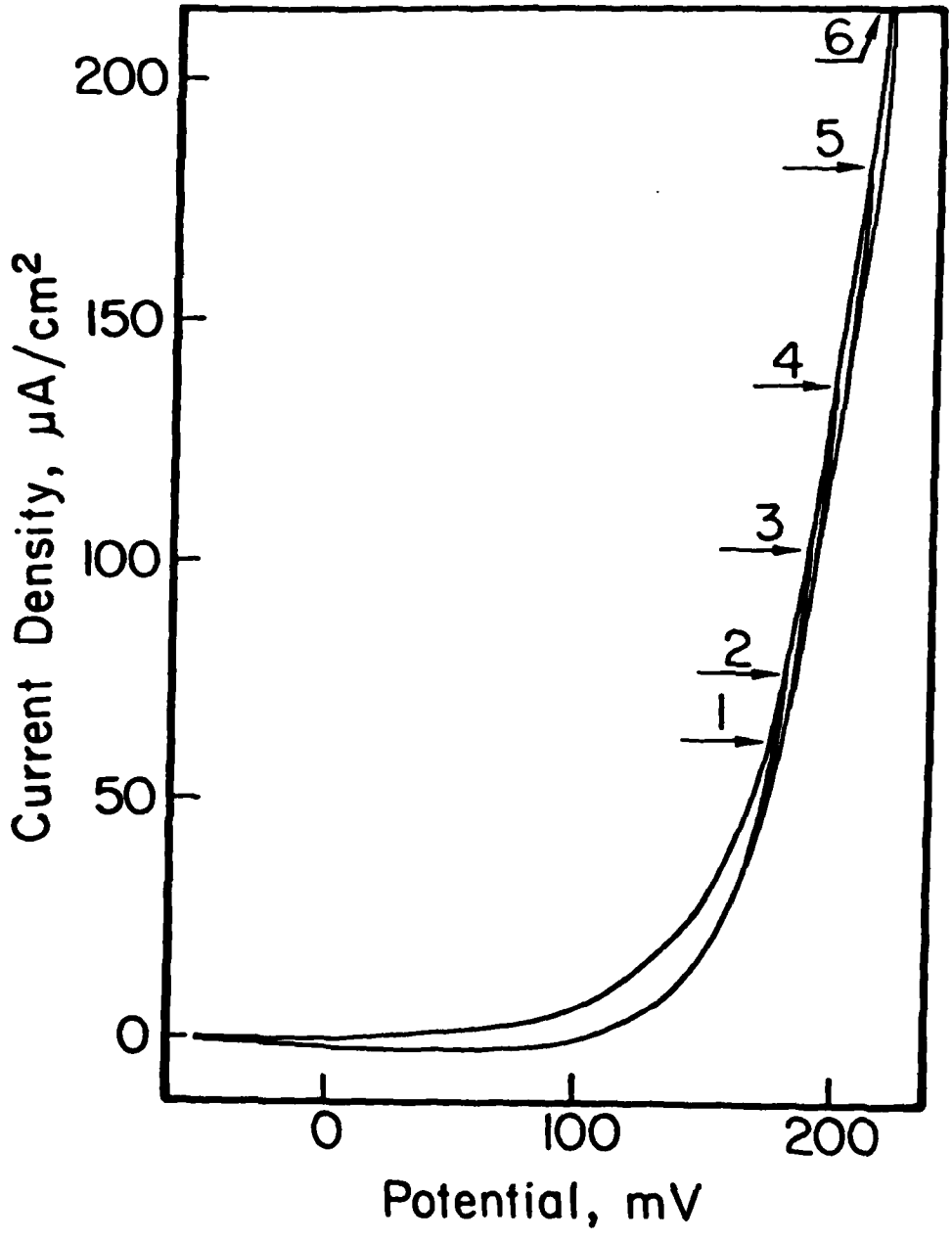
Current Density, μA/cm²
200
150
100
50
0
0
100
200
Potential, mV
1
2
3
4
5
6

Fig. 6.

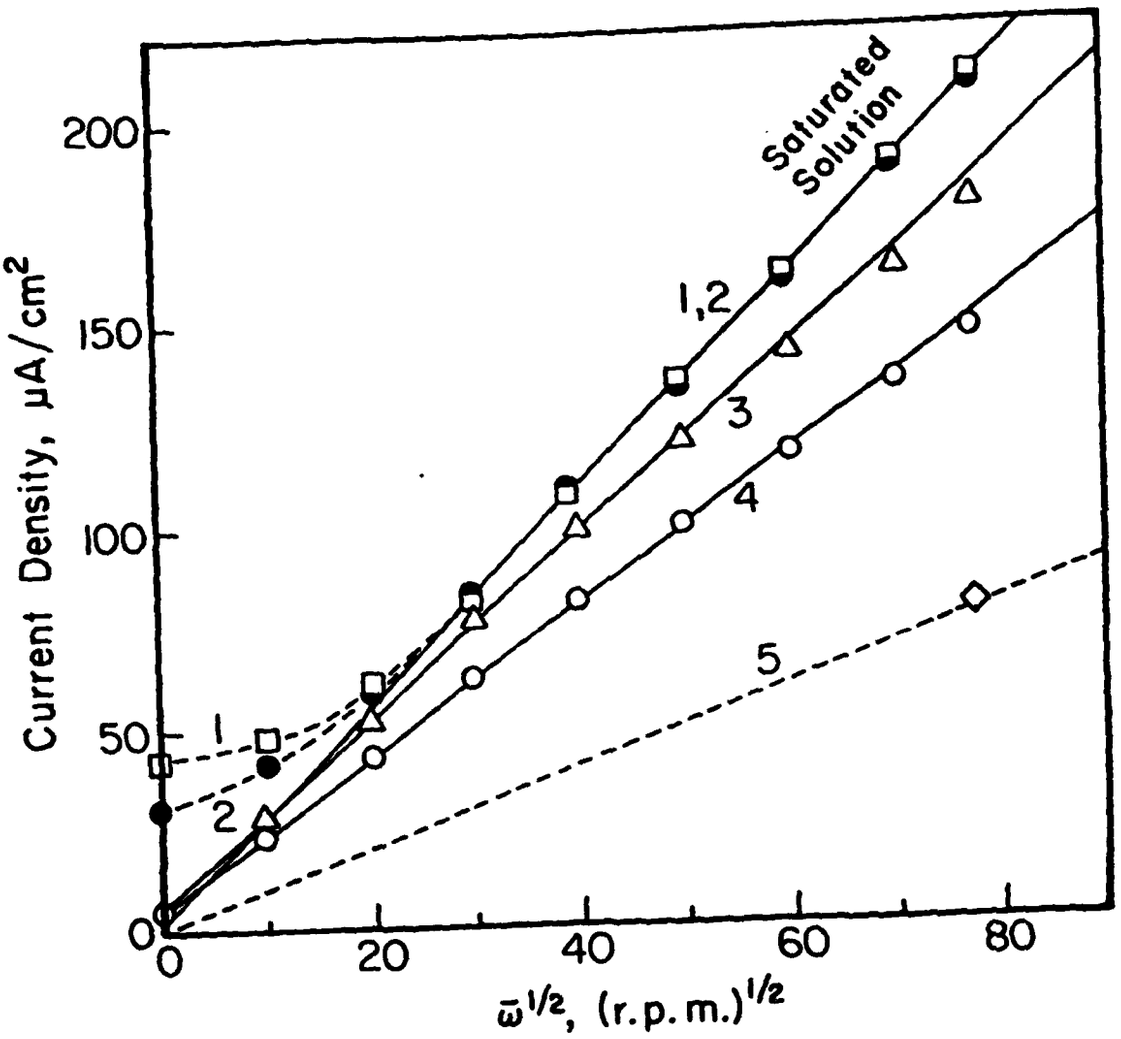
Saturated Solution
1,2
3
4
5
1
2
Current Density, μA/cm²
ω^1/2, (r.p.m.)^1/2
0
50
100
150
200
0
20
40
60
80

Fig. 7

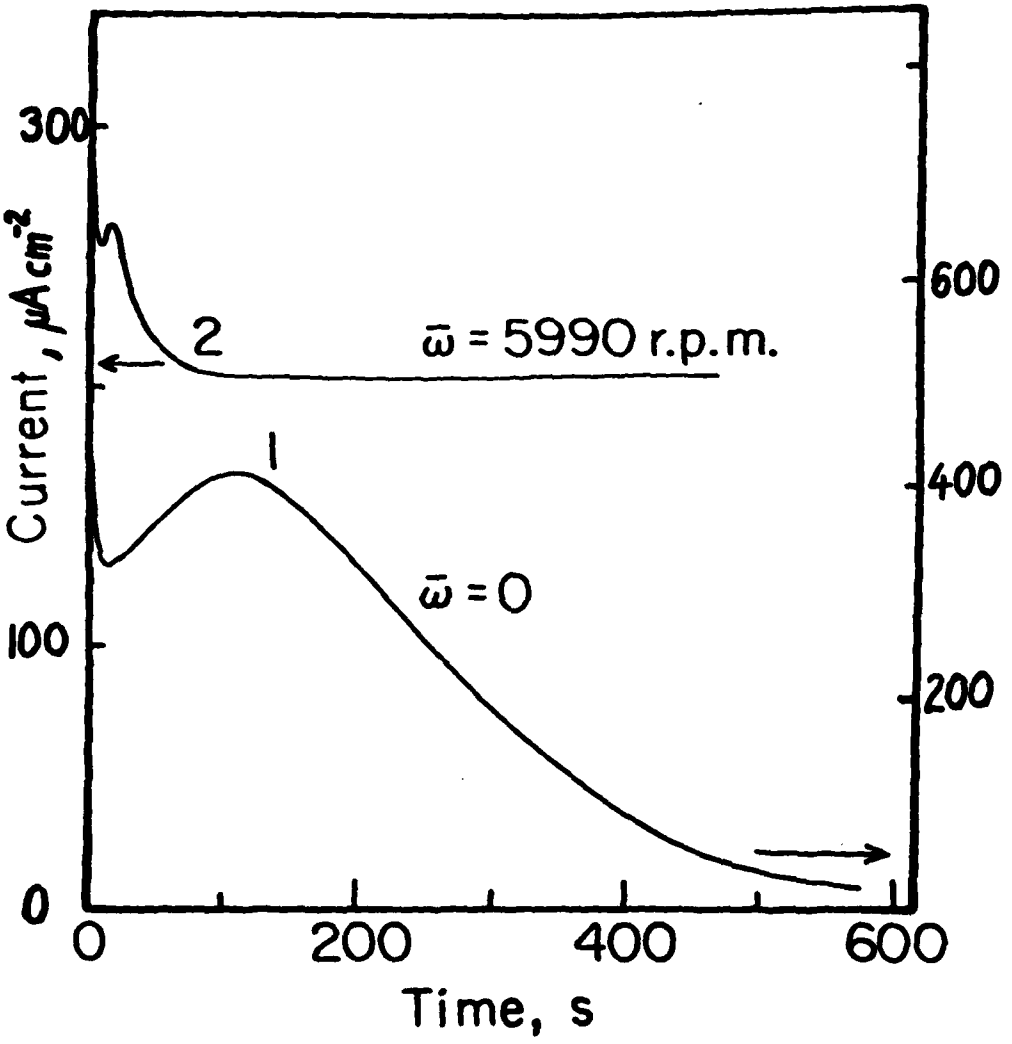
300
100
0
Current, μAcm⁻²
2
ω̄ = 5990 r.p.m.
1
ω̄ = 0
600
400
200
0
200
400
600
Time, s

Fig. 8

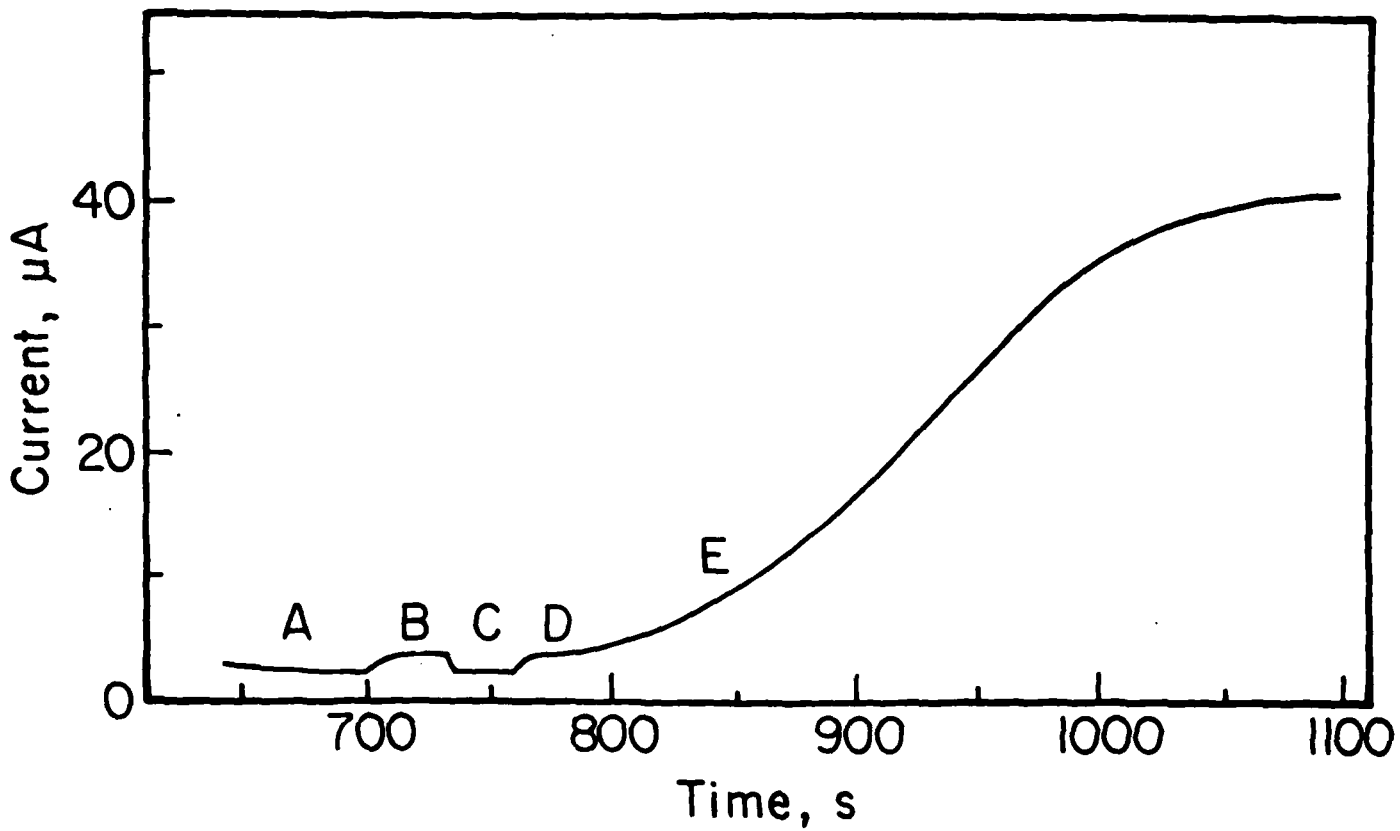

Fig. 5

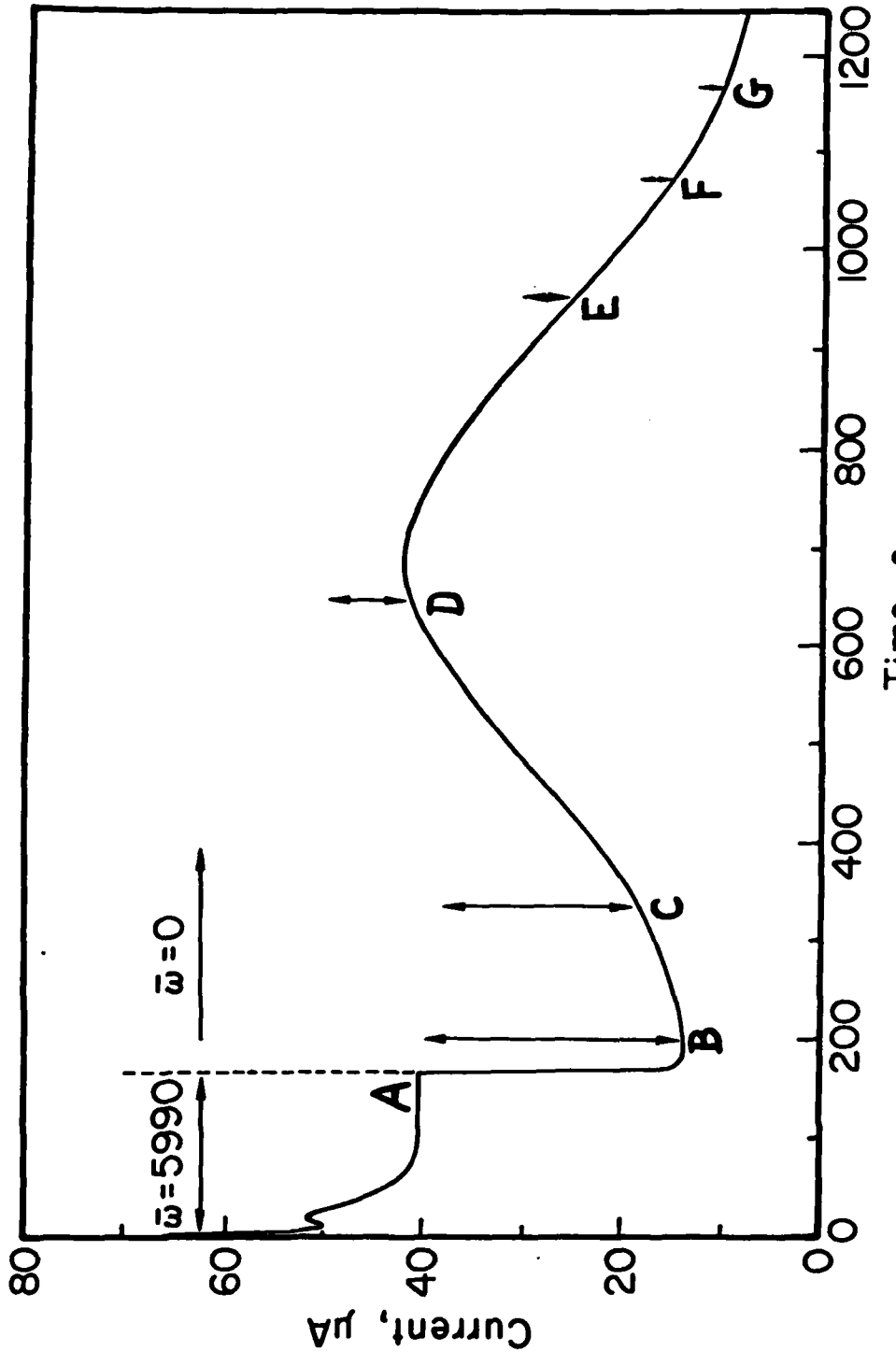
Current, μA
Time, s
0
20
40
60
80
200
400
600
800
1000
1200
A
B
C
D
E
F
G
ω=5990
ω=0

Fig. 10

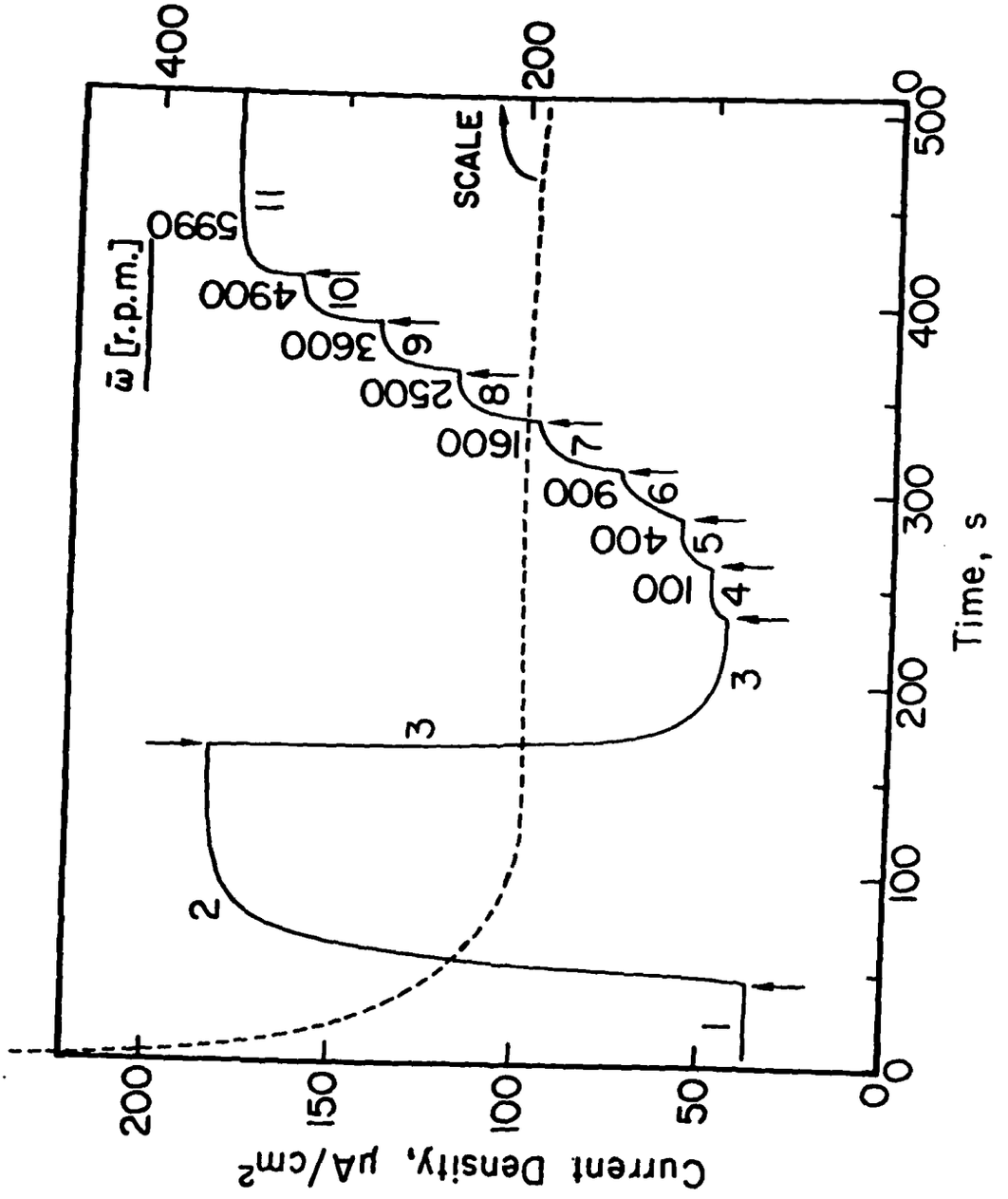
Current Density, μA/cm²
Time, s
SCALE
ω̄ [r.p.m.]
5990
4900
3600
2500
1600
900
400
100
1
2
3
4
5
6
7
8
9
10
11

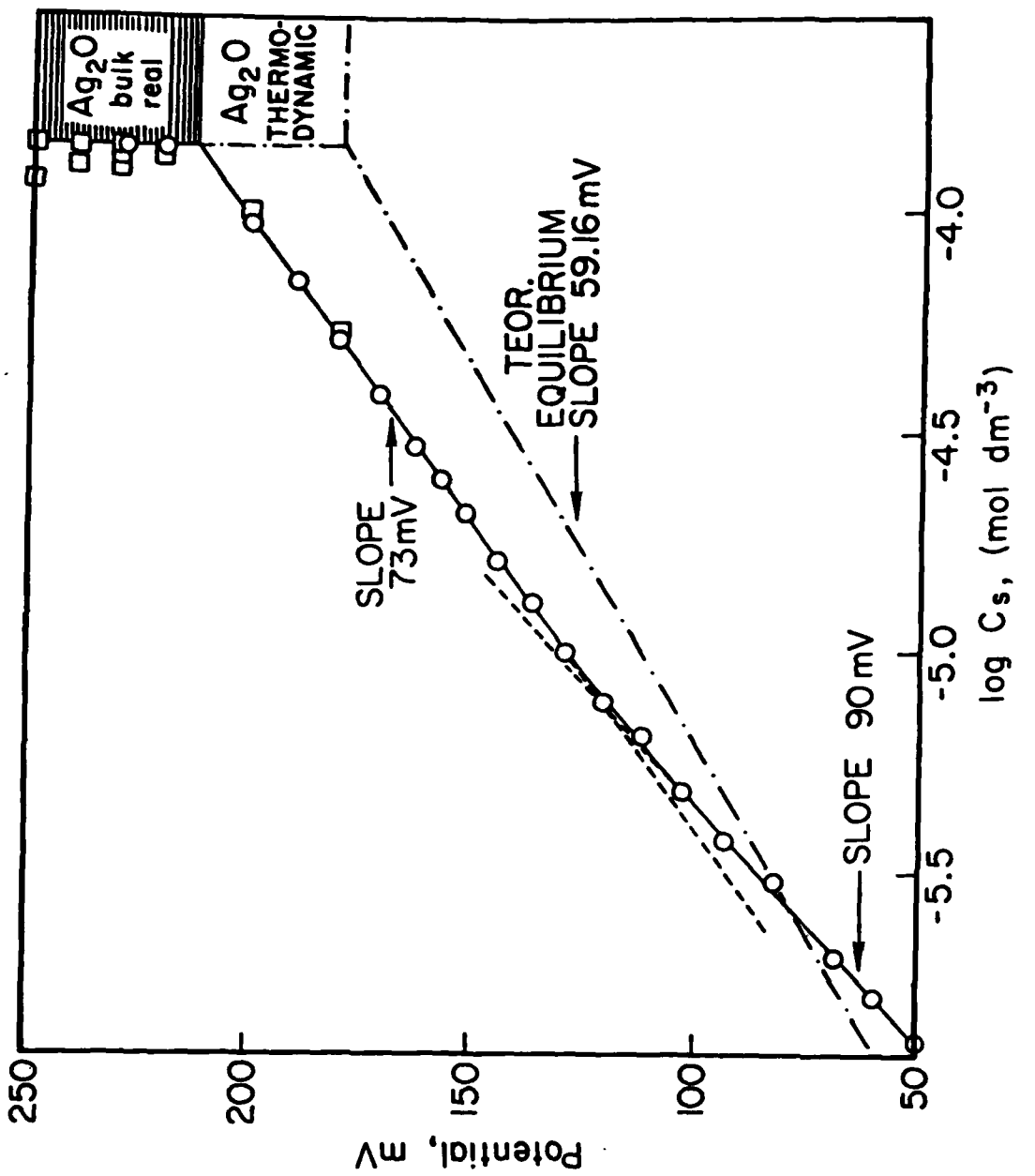
Potential, mV
250
200
150
100
50
-5.5
-5.0
-4.5
-4.0
log C_s, (mol dm^{-3})
Ag_2O bulk real
Ag_2O THERMO-DYNAMIC
TEOR. EQUILIBRIUM SLOPE 59.16mV
SLOPE 73mV
SLOPE 90mV

Fig. 12

TECHNICAL REPORT DISTRIBUTION LIST, GEN

	No. Copies
Office of Naval Research Attn: Code 413 800 N. Quincy Street Arlington, Virginia 22217	2
ONR Pasadena Detachment Attn: Dr. R. J. Marcus 1030 East Green Street Pasadena, California 91106	1
Commander, Naval Air Systems Command Attn: Code 310C (H. Rosenwasser) Washington, D.C. 20360	1
Naval Civil Engineering Laboratory Attn: Dr. R. W. Drisko Port Hueneme, California 93401	1
Superintendent Chemistry Division, Code 6100 Naval Research Laboratory Washington, D.C. 20375	1
Defense Technical Information Center Building 5, Cameron Station Alexandria, Virginia 22314	12
DTNSRDC Attn: Dr. G. Bosmajian Applied Chemistry Division Annapolis, Maryland 21401	1
Naval Ocean Systems Center Attn: Dr. S. Yamamoto Marine Sciences Division San Diego, California 91232	1
Naval Ocean Systems Center Attn: Technical Library San Diego, California 92152	1
Naval Weapons Center Attn: Dr. A. B. Amster Chemistry Division China Lake, California 93555	1
Scientific Advisor Commandant of the Marine Corps Code RD-1 Washington, D.C. 20380	1
Dean William Tolles Naval Postgraduate School Monterey, California 93940	1
U.S. Army Research Office Attn: CRD-AA-IP P.O. Box 12211 Research Triangle Park, NC 27709	1
Mr. Vincent Schaper DTNSRDC Code 2830 Annapolis, Maryland 21402	1
Mr. John Boyle Materials Branch Naval Ship Engineering Center Philadelphia, Pennsylvania 19112	1
Mr. A. M. Anzalone Administrative Librarian PLASTEC/ARRADCOM Bldg 3401 Dover, New Jersey 07801	1

TECHNICAL REPORT DISTRIBUTION LIST, 359

Dr. Paul Delahay
Department of Chemistry
New York University
New York, New York 10003

Dr. P. J. Hendra
Department of Chemistry
University of Southampton
Southampton S09 5NH
United Kingdom

Dr. T. Katan
Lockheed Missiles and
Space Co., Inc.
P.O. Box 504
Sunnyvale, California 94088

Dr. D. N. Bennion
Department of Chemical Engineering
Brighma Young University
Provo, Utah 84602

Dr. R. A. Marcus
Department of Chemistry
California Institute of Technology
Pasadena, California 91125

Mr. Joseph McCartney
Code 7121
Naval Ocean Systems Center
San Diego, California 92152

Dr. J. J. Auborn
Bell Laboratories
Murray Hill, New Jersey 07974

Dr. Joseph Singer, Code 302-1
NASA-Lewis
21000 Brookpark Road
Cleveland, Ohio 44135

Dr. P. P. Schmidt
Department of Chemistry
Oakland University
Rochester, Michigan 48063

Dr. H. Richtol
Chemistry Department
Rensselaer Polytechnic Institute
Troy, New York 12181

Dr. E. Yeager
Department of Chemistry
Case Western Reserve University
Cleveland, Ohio 44106

Dr. C. E. Mueller
The Electrochemistry Branch
Naval Surface Weapons Center
White Oak Laboratory
Silver Spring, Maryland 20910

Dr. Sam Perone
Chemistry & Materials
Science Department
Lawrence Livermore National Lab.
Livermore, California 94550

Dr. Royce W. Murray
Department of Chemistry
University of North Carolina
Chapel Hill, North Carolina 27514

Dr. G. Goodman
Johnson Controls
5757 North Green Bay Avenue
Milwaukee, Wisconsin 53201

Dr. B. Brummer
EIC Incorporated
111 Chapel Street
Newton, Massachusetts 02158

Dr. Adam Heller
Bell Laboratories
Murray Hill, New Jersey 07974

Electrochimica Corporation
Attn: Technical Library
2485 Charleston Road
Mountain View, California 94040

Library
Duracell, Inc.
Burlington, Massachusetts 01803

Dr. A. B. Ellis
Chemistry Department
University of Wisconsin
Madison, Wisconsin 53706

TECHNICAL REPORT DISTRIBUTION LIST, 359

Dr. M. Wrighton
Chemistry Department
Massachusetts Institute
of Technology
Cambridge, Massachusetts 02139

Dr. B. Stanley Pons
Department of Chemistry
University of Utah
Salt Lake City, Utah 84112

Donald E. Mains
Naval Weapons Support Center
Electrochemical Power Sources Division
Crane, Indiana 47522

S. Ruby
DOE (STOR)
M.S. 6B025 Forrestal Bldg.
Washington, D.C. 20595

Dr. A. J. Bard
Department of Chemistry
University of Texas
Austin, Texas 78712

Dr. Janet Osteryoung
Department of Chemistry
State University of New York
Buffalo, New York 14214

Dr. Donald W. Ernst
Naval Surface Weapons Center
Code R-33
White Oak Laboratory
Silver Spring, Maryland 20910

Mr. James R. Moden
Naval Underwater Systems Center
Code 3632
Newport, Rhode Island 02840

Dr. Bernard Spielvogel
U.S. Army Research Office
P.O. Box 12211
Research Triangle Park, NC 27709

Dr. William Ayers
ECD Inc.
P.O. Box 5357
North Branch, New Jersey 08876

Dr. M. M. Nicholson
Electronics Research Center
Rockwell International
3370 Miraloma Avenue
Anaheim, California

Dr. Michael J. Weaver
Department of Chemistry
Purdue University
West Lafayette, Indiana 47907

Dr. R. David Rauh
EIC Corporation
111 Chapel Street
Newton, Massachusetts 02158

Dr. Aaron Wold
Department of Chemistry
Brown University
Providence, Rhode Island 02192

Dr. Martin Fleischmann
Department of Chemistry
University of Southampton
Southampton SO9 5NH ENGLAND

Dr. R. A. Osteryoung
Department of Chemistry
State University of New York
Buffalo, New York 14214

Dr. Denton Elliott
Air Force Office of Scientific
Research
Bolling AFB
Washington, D.C. 20332

Dr. R. Nowak
Naval Research Laboratory
Code 6130
Washington, D.C. 20375

Dr. D. F. Shriver
Department of Chemistry
Northwestern University
Evanston, Illinois 60201

Dr. Aaron Fletcher
Naval Weapons Center
Code 3852
China Lake, California 93555

TECHNICAL REPORT DISTRIBUTION LIST, 359

Dr. David Aikens
Chemistry Department
Rensselaer Polytechnic Institute
Troy, New York 12181

Dr. A. P. B. Lever
Chemistry Department
York University
Downsview, Ontario M3J1P3

Dr. Stanislaw Szpak
Naval Ocean Systems Center
Code 6343, Bayside
San Diego, California 95152

Dr. Gregory Farrington
Department of Materials Science
and Engineering
University of Pennsylvania
Philadelphia, Pennsylvania 19104

M. L. Robertson
Manager, Electrochemical
and Power Sources Division
Naval Weapons Support Center
Crane, Indiana 47522

Dr. T. Marks
Department of Chemistry
Northwestern University
Evanston, Illinois 60201

Dr. Micha Tomkiewicz
Department of Physics
Brooklyn College
Brooklyn, New York 11210

Dr. Lesser Blum
Department of Physics
University of Puerto Rico
Rio Piedras, Puerto Rico 00931

Dr. Joseph Gordon, II
IBM Corporation
K33/281
5600 Cottle Road
San Jose, California 95193

Dr. D. H. Whitmore
Department of Materials Science
Northwestern University
Evanston, Illinois 60201

Dr. Alan Bewick
Department of Chemistry
The University of Southampton
Southampton, SO9 5NH ENGLAND

Dr. E. Anderson
NAVSEA-56Z33 NC #4
2541 Jefferson Davis Highway
Arlington, Virginia 20362

Dr. Bruce Dunn
Department of Engineering &
Applied Science
University of California
Los Angeles, California 90024

Dr. Elton Cairns
Energy & Environment Division
Lawrence Berkeley Laboratory
University of California
Berkeley, California 94720

Dr. D. Cipris
Allied Corporation
P.O. Box 3000R
Morristown, New Jersey 07960

Dr. M. Philpott
IBM Corporation
5600 Cottle Road
San Jose, California 95193

Dr. Donald Sandstrom
Department of Physics
Washington State University
Pullman, Washington 99164

Dr. Carl Kannewurf
Department of Electrical Engineering
and Computer Science
Northwestern University
Evanston, Illinois 60201

TECHNICAL REPORT DISTRIBUTION LIST, 359

Dr. Robert Somoano
Jet Propulsion Laboratory
California Institute of Technology
Pasadena, California 91103

Dr. Johann A. Joebstl
USA Mobility Equipment R&D Command
DRDME-EC
Fort Belvoir, Virginia 22060

Dr. Judith H. Ambrus
NASA Headquarters
M.S. RTS-6
Washington, D.C. 20546

Dr. Albert R. Landgrebe
U.S. Department of Energy
M.S. 6B025 Forrestal Building
Washington, D.C. 20595

Dr. J. J. Brophy
Department of Physics
University of Utah
Salt Lake City, Utah 84112

Dr. Charles Martin
Department of Chemistry
Texas A&M University
College Station, Texas 77843

Dr. H. Tachikawa
Department of Chemistry
Jackson State University
Jackson, Mississippi 39217

Dr. Theodore Beck
Electrochemical Technology Corp.
3935 Leary Way N.W.
Seattle, Washington 98107

Dr. Farrell Lytle
Boeing Engineering and
Construction Engineers
P.O. Box 3707
Seattle, Washington 98124

Dr. Robert Gotscholl
U.S. Department of Energy
MS G-226
Washington, D.C. 20545

Dr. Edward Fletcher
Department of Mechanical Engineering
University of Minnesota
Minneapolis, Minnesota 55455

Dr. John Fontanella
Department of Physics
U.S. Naval Academy
Annapolis, Maryland 21402

Dr. Martha Greenblatt
Department of Chemistry
Rutgers University
New Brunswick, New Jersey 08903

Dr. John Wasson
Syntheco, Inc.
Rte 6 - Industrial Pike Road
Gastonia, North Carolina 28052

Dr. Walter Roth
Department of Physics
State University of New York
Albany, New York 12222

Dr. Anthony Sammells
Eltron Research Inc.
710 E. Ogden Avenue #108
Naperville, Illinois 60540

Dr. W. M. Risen
Department of Chemistry
Brown University
Providence, Rhode Island 02192

Dr. C. A. Angell
Department of Chemistry
Purdue University
West Lafayette, Indiana 47907

Dr. Thomas Davis
Polymer Science and Standards
Division
National Bureau of Standards
Washington, D.C. 20234

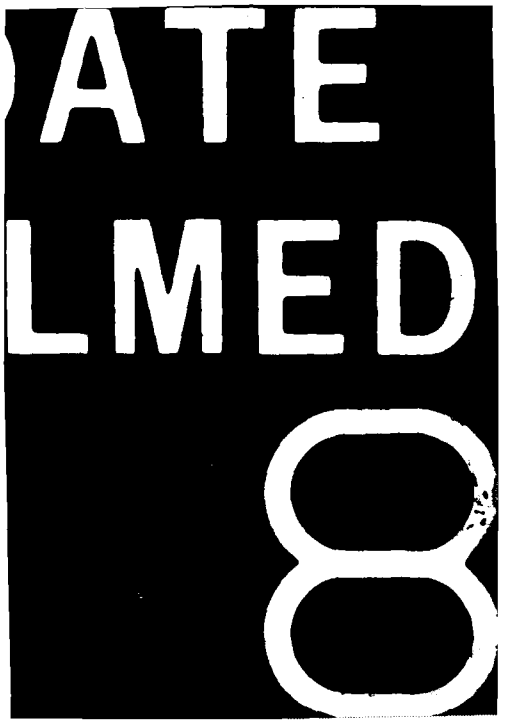
ATE
LMED
8